

## On-chip, high-sensitivity temperature sensors based on dye-doped solid-state polymer microring lasers

Lei Wan,<sup>1,2,a)</sup> Hengky Chandrahali,<sup>3,a)</sup> Cong Chen,<sup>1,4,a)</sup> Qiushu Chen,<sup>3</sup> Ting Mei,<sup>5</sup> Yuji Oki,<sup>4</sup> Naoya Nishimura,<sup>6</sup> L. Jay Guo,<sup>1,b)</sup> and Xudong Fan<sup>3,b)</sup>

<sup>1</sup>Department of Electrical Engineering and Computer Science, University of Michigan, Ann Arbor, Michigan 48109, USA

<sup>2</sup>Institute of Optoelectronic Material and Technology, South China Normal University, Guangzhou 510631, China

<sup>3</sup>Department of Biomedical Engineering, University of Michigan, Ann Arbor, Michigan 48109, USA

<sup>4</sup>Graduate School and Faculty of Information Science and Electrical Engineering, Kyushu University, Fukuoka 819-0395, Japan

<sup>5</sup>School of Science, Northwestern Polytechnical University, Xi'an 710072, China

<sup>6</sup>Nissan Chemical Industries, Ltd., 488-6, Suzumi-cho, Funabashi 274-0052, Japan

(Received 7 June 2017; accepted 1 August 2017; published online 10 August 2017)

We developed a chip-scale temperature sensor with a high sensitivity of 228.6 pm/°C based on a rhodamine 6G (R6G)-doped SU-8 whispering gallery mode microring laser. The optical mode was largely distributed in a polymer core layer with a 30 μm height that provided detection sensitivity, and the chemically robust fused-silica microring resonator host platform guaranteed its versatility for investigating different functional polymer materials with different refractive indices. As a proof of concept, a dye-doped hyperbranched polymer (TZ-001) microring laser-based temperature sensor was simultaneously developed on the same host wafer and characterized using a free-space optics measurement setup. Compared to TZ-001, the SU-8 polymer microring laser had a lower lasing threshold and a better photostability. The R6G-doped SU-8 polymer microring laser demonstrated greater adaptability as a high-performance temperature-sensing element. In addition to the sensitivity, the temperature resolutions for the laser-based sensors were also estimated to be 0.13 °C and 0.35 °C, respectively. The rapid and simple implementation of micrometer-sized temperature sensors that operate in the range of 31–43 °C enables their potential application in thermometry.

Published by AIP Publishing. [<http://dx.doi.org/10.1063/1.4986825>]

Sensitive temperature sensing is a significant driving force behind the development of thermometry technologies in a variety of important fields, such as in biological treatments<sup>1</sup> and medical diagnosis.<sup>2,3</sup> A suitable biocompatible temperature sensor at the micro- and nanoscale could determine the effects of temperature-related metabolic activities on living cells. Recently, different nanothermometers based on temperature-dependent optical properties, such as a photoluminescent nanothermometer composed of polymer-encapsulated quantum dots (P-QD),<sup>4</sup> a green fluorescent probe based on NaYF<sub>4</sub>:Er<sup>3+</sup>, Yb<sup>3+</sup> nanoparticles,<sup>5</sup> and a thermoresponsive poly(*N*-isopropylacrylamide) (pNIPAM)-coated optical microfiber,<sup>6</sup> were employed to detect environmental temperatures at cellular levels in the temperature range of human organs of 35–42 °C. However, most of the temperature sensors mentioned above have low sensitivities and are difficult to modify for on-chip integration, which is typically used for multifunctional biological monitoring and treatment. Therefore, development of chip-scale integrated temperature sensors with high sensitivities is highly desirable.

Given their unique characteristics that include easy integration, rapid response time, and immunity to electromagnetic radiation,<sup>7–9</sup> passive optical whispering gallery mode (WGM) resonators with high Q-factors and small mode

volumes have attracted significant attention as common sensing units in the past decade. In general, these resonator geometries could be fabricated on chips using different host materials, including silicon,<sup>10</sup> silica,<sup>11,12</sup> and polymer.<sup>13</sup> The spectral position of the WGM resonance is affected by the thermal-optic (TO) and thermal expansion (TE) effects of the resonator materials and surrounding environment, which has been extensively explored for temperature sensing applications.<sup>14–16</sup> For instance, because of the compatibility with CMOS fabrication processes, silicon-based temperature sensors are preferred due to their excellent thermal conductivity [ $\sim 149$  W/(m·K)].<sup>17–20</sup> However, the sensitivity of a pure silicon ring resonator-based temperature sensor is limited to approximately 80 pm/°C due to the low TO coefficient of silicon ( $\sim 1.8 \times 10^{-4}$  K<sup>-1</sup>).<sup>21–23</sup> Silica is another material that is commonly used to fabricate ring resonators, but silica has an even lower TO coefficient ( $\sim 1 \times 10^{-5}$  K<sup>-1</sup>)<sup>24</sup> and temperature sensitivity. To improve the sensitivity, a silica ring resonator was recently coated with a layer of polydimethylsiloxane, and a sensitivity of 151 pm/°C was achieved.<sup>25</sup> In nearly all passive WGM resonator-based temperature sensors, the resonance probing and readout are realized using an optical fiber taper, a waveguide, or a prism, which not only requires sub-micrometer precision positioning but also makes the entire device cumbersome and susceptible to mechanical vibrations.<sup>26,27</sup>

For an active resonator-based temperature sensor, the measurement setup is simpler because free-space optics can be

<sup>a)</sup>L. Wan, H. Chandrahali, and C. Chen contributed equally to this work.

<sup>b)</sup>Authors to whom correspondence should be addressed: guo@umich.edu; xsfan@umich.edu

employed to probe the WGM spectral position. Furthermore, gain media can reduce the spectral linewidth and improve the detection limit of an active resonator-based temperature sensor.<sup>28,29</sup> To this end, in our work, an organic dye R6G-doped polymer SU-8 was deposited as a gain medium on the fused-silica microring resonator host wafer to fabricate an SU-8 laser-based temperature sensor. To demonstrate the versatility of our microring resonator host platform, the R6G-doped hyperbranched polymer TZ-001<sup>30</sup> was deposited as another gain material on the same wafer to create a TZ-001 laser-based temperature sensor with different temperature-dependent characteristics. In the experiments, different optical properties, including the spectral characteristics, lasing thresholds, and photostability of both polymer microring lasers, were separately characterized and compared to estimate the feasibility of their use as temperature sensing elements.

The solid-state polymer microring laser-based temperature sensor used in this work consisted of a fused-silica microring resonator host with a channel profile as a cladding layer and a cured R6G-doped polymer gain material deposited on it as a core layer. Figure 1 illustrates the top and cross-sectional views of the active WGMs resonator-based temperature sensor. Figure 2(a) depicts the scanning electron microscope (SEM) image of an etched fused-silica microring resonator host prior to polymer deposition. The detailed fabrication processes were presented in our previous work.<sup>31</sup> The fabrication methods of the solid-state polymer core layer are displayed in Figs. 2(b)–2(d). A free-space optics measurement system is provided in Fig. 3 (details are shown in the supplementary material).

Figure 4(a) depicts the lasing spectral characteristics of an R6G-doped SU-8 solid-state polymer microring laser. The full width at half maximum (FWHM) of the lasing peak at approximately 597.567 nm was measured to be 0.034 nm, which was limited by the spectrometer's spectral resolution ( $\sim 0.03$  nm). Using the equation for the Q-factor of a passive resonator ( $Q = \lambda/\Delta\lambda$ ),<sup>32</sup> the corresponding Q-factor for this R6G-doped polymer microring laser was estimated to be  $1.76 \times 10^4$ . We have previously measured the Q-factor of a passive ring resonator from the same fabrication batch<sup>33</sup> and observed a comparable Q-factor. In addition, we have also measured laser emissions from various fluidic gain media that fill the entire ring resonator host<sup>34</sup> and recorded a comparable laser linewidth. Therefore, we conclude there was no noticeable additional scattering loss originated from the gain film in our current device. The free spectrum range (FSR)

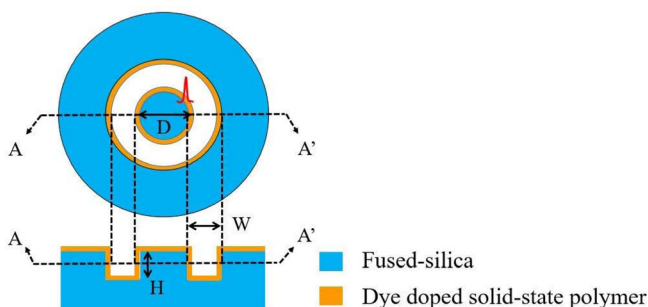


FIG. 1. Top view and cross-sectional view along the AA' plane of a dye-doped solid-state polymer microring laser.

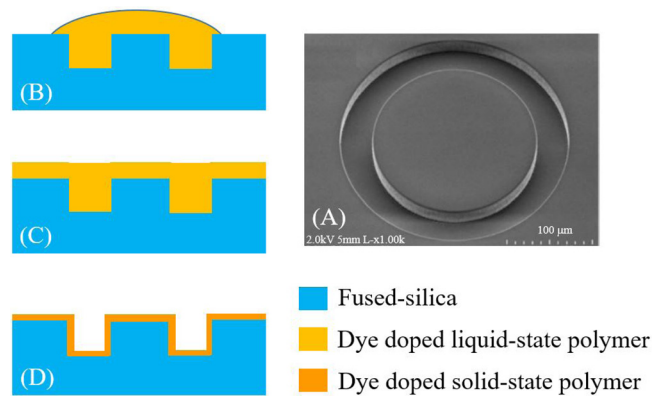


FIG. 2. (a) SEM image of an etched fused-silica microring resonator host with a channel profile. The width (W) and height (H) of this ring resonator host were  $40 \mu\text{m}$  and  $30 \mu\text{m}$ , respectively. The diameter (D) of the inner fused-silica microdisc was  $220 \mu\text{m}$ . (b)–(d) Cross-sectional views corresponding to a dye-doped liquid-state polymer (b) dripped, (c) spin-coated, and (d) cured on the patterned wafer.

was measured to be 0.3 nm, the refractive index of the SU-8 was estimated to be 1.6, which corresponds to the radius of the microring laser of approximately  $115.4 \mu\text{m}$ , suggesting that the scattered lasing signals came mainly from the inner microring resonator. The thickness of the SU-8 polymer can be further estimated to be  $5.4 \mu\text{m}$ .

To further investigate the feasibility of an R6G-doped SU-8 polymer microring laser as a high-performance temperature sensor, the lasing threshold and photostability of the polymer laser were characterized. The lasing threshold was determined to be  $1.28 \mu\text{J}/\text{mm}^2$ , as shown in Fig. 5(a). The laser photostability was investigated under an intermittent pump mechanism. Figure 6(a) illustrates that the lasing spectra were obtained under a pump intensity of  $75.7 \mu\text{J}/\text{mm}^2$ , which is approximately 60 times the lasing threshold. These lasing spectra were collected over ten measurements with a 30 s interval between adjacent measurements, and they indicate that

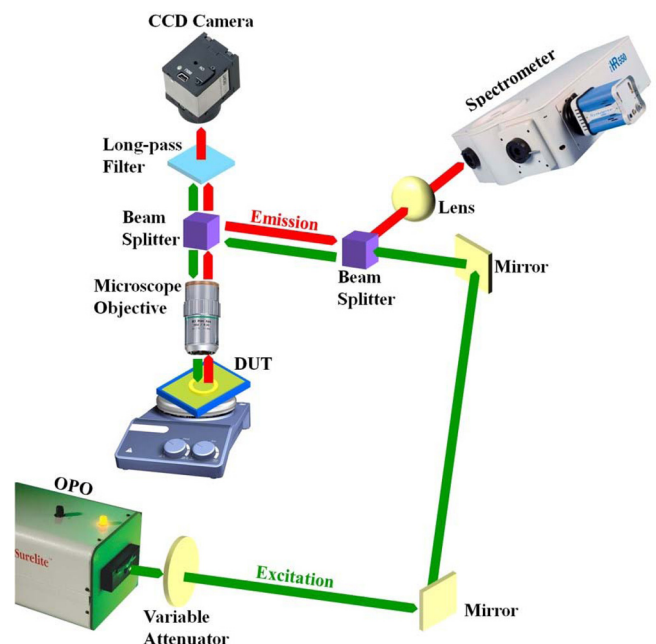


FIG. 3. Illustration of the measurement setup for the dye-doped solid-state polymer microring resonator laser-based temperature sensor.

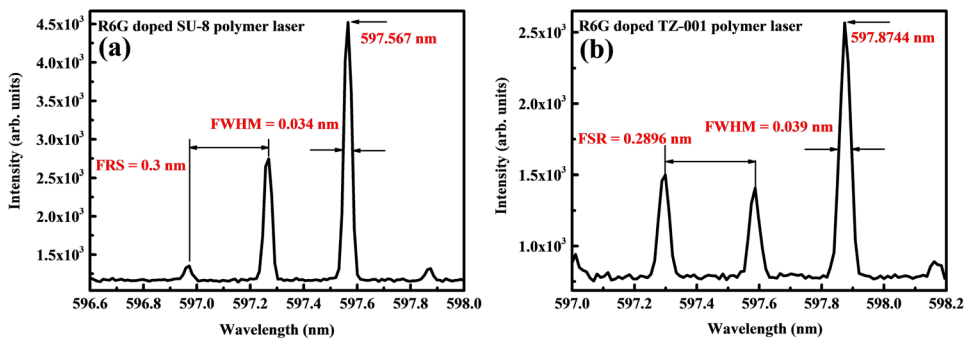


FIG. 4. Comparison of the lasing spectral characteristics between (a) R6G-doped SU-8 polymer microring laser and (b) R6G-doped TZ-001 polymer microring laser.

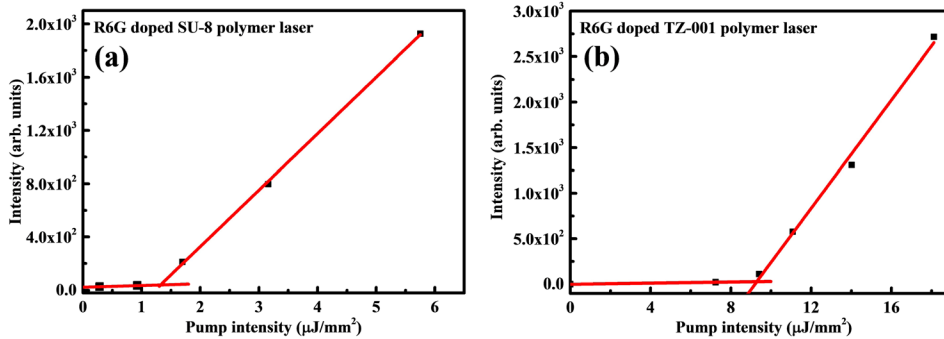


FIG. 5. Comparison of the lasing thresholds between (a) R6G-doped SU-8 polymer microring laser and (b) R6G-doped TZ-001 polymer microring laser.

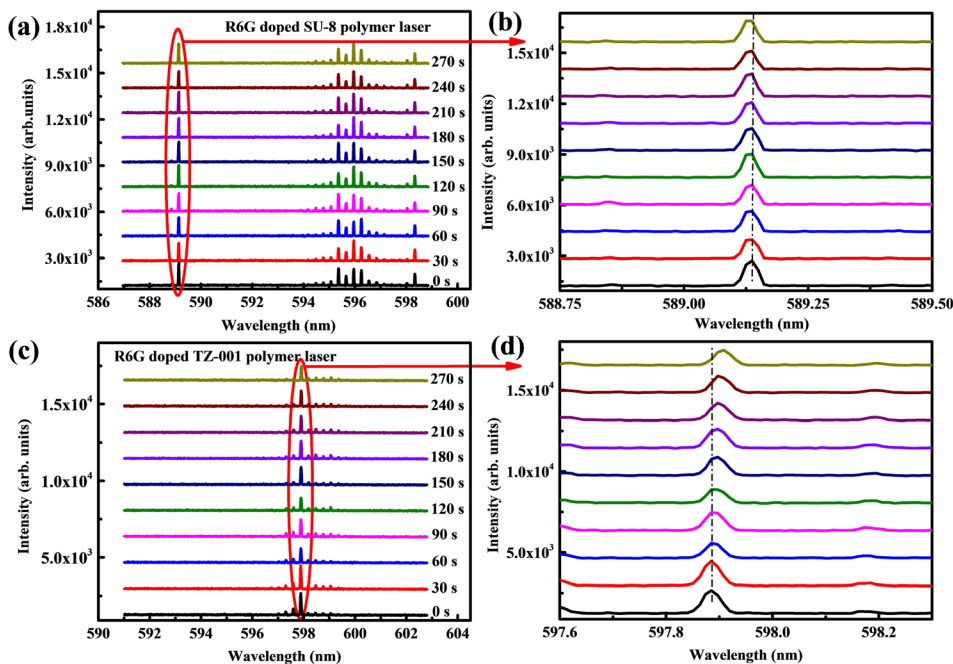


FIG. 6. Lasing spectra collected under different time intervals for the R6G-doped (a) SU-8 polymer microring laser and (c) TZ-001 polymer microring laser. Expansion of the lasing spectra at approximately 589.12 nm for (b) SU-8 and at approximately 597.9 nm for (d) TZ-001.

the SU-8 polymer microring laser had good photostability. Detailed studies in Fig. 6(b) using the lasing peak at 589.12 nm as the spectral marker exhibited a total spectral shift of less than 0.011 nm even under an extremely high pump intensity.

Temperature sensing by the R6G-doped solid-state polymer microring laser was achieved by measuring the lasing peak shift that resulted from the TO and TE effects of the resonator materials, as explained in the following equation:

$$d\lambda = \lambda \left( \frac{1}{n_{\text{eff}}} \frac{dn_{\text{eff}}}{dT} + \frac{1}{D} \frac{dD}{dT} \right) dT, \quad (1)$$

where  $D$  is the diameter of the polymer microring resonator and  $n_{\text{eff}}$  is the effective refractive index of the polymer

microring resonator.  $dn_{\text{eff}}/dT$  and  $\frac{1}{D} \frac{dD}{dT}$  denote the TO coefficient and the TE coefficient of the resonator material, respectively. During the experiment, the hot plate temperature was changed from 31 °C to 43 °C, which covers the physiological temperature range of 35 °C to 42 °C. As illustrated in Fig. 7(a), a 0.92 nm blue-shift in the lasing peak was observed when the temperature increased from 39 °C to 43 °C, which is mainly attributed to the negative TO coefficient of the polymer SU-8 ( $\sim -3.5 \times 10^{-4} \text{K}^{-1}$ )<sup>24</sup> because the TE coefficient of the solid SU-8 material ( $\sim 10^{-6} \text{K}^{-1}$ )<sup>35</sup> is negligible compared to the TO coefficient.

By linearly fitting the experimental data, the sensitivity of the temperature sensor was determined to be 0.2286 nm/°C [Fig. 7(b)]. Compared to the previous ring resonator-based

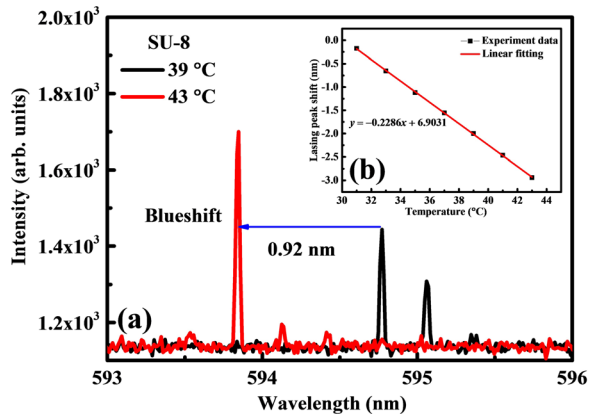


FIG. 7. (a) Lasing spectra of the R6G-doped SU-8 polymer microring laser at 39 °C and 43 °C. (b) The inset depicts the lasing peak shifts as a linear function of temperature.

temperature sensors,<sup>17–19,25</sup> the sensor reported in this work has a higher temperature sensitivity while avoiding the use of cumbersome and delicate fiber taper or waveguide coupling (see Table SI in [supplementary material](#)). The sensitivity of the temperature sensor in our work was significantly enhanced because the optical mode distribution was largely confined in the approximately 30  $\mu\text{m}$  height of the SU-8 core layer of the polymer microring resonator. Compared to the passive silicon ring resonator-based temperature sensor reported by Kim *et al.*,<sup>17</sup> the SU-8 polymer microring laser-based temperature sensor was three times more sensitive and its linewidth was twice as narrow. Theoretically, the temperature resolution could be improved to 6 times that of the silicon resonator (i.e.,  $\sim 1.67 \times 10^{-3} \text{ }^\circ\text{C}$ ). However, in practice, due to the limitation of the spectrometer resolution, the detection limit of this temperature sensor was estimated to be approximately 0.13 °C. The realization of the SU-8 polymer microring laser-based temperature sensor with a micrometer-sized footprint thereby demonstrates its capability for high-sensitivity temperature sensing.

As a significant advantage, the chemical robustness of the fused-silica resonator host platform guarantees its versatility with functional polymer materials with different refractive indices. In the design and fabrication of miniaturized polymer resonator devices, optical polymer materials with high refractive indices are always selected to create a large contrast in the refractive index. This is one reason we employed polymer TZ-001, which has a high refractive index of 1.78, as a gain carrier. Furthermore, as a hyperbranched polymer, the studies in this work could advance the knowledge of the physical and mechanical properties of TZ-001.

Figure 4(b) depicts the lasing spectral characteristics of an R6G-doped TZ-001 polymer microring laser. The FWHM is similar to that of SU-8, but the FSR is smaller due to the higher refractive index of TZ-001. Based on the FSR, the radius of the R6G-doped TZ-001 polymer microring laser was estimated to be 110.5  $\mu\text{m}$ , indicating that the TZ-001 layer (0.5  $\mu\text{m}$ ) was significantly thinner than SU-8 as a result of the need to deposit the brittle TZ-001 under a higher spin-speed than SU-8 to avoid potential cracks that may occur during low-speed deposition.

Similarly, the lasing threshold was measured to be 9.28  $\mu\text{J}/\text{mm}^2$  [Fig. 5(b)], which suggests that the TZ-001

polymer microring laser had a lower Q-factor than SU-8. This was mainly attributed to the large scattering loss resulting from the brittle TZ-001 core layer polymer. The photostability of the lasing spectra was observed at different time intervals under a pump intensity of 140  $\mu\text{J}/\text{mm}^2$  [Fig. 6(c)]. Figure 6(d) indicates that a redshift of approximately 0.02 nm occurred from 0 s to 270 s time intervals. This might be caused by photobleaching resulting from the large pump intensity applied.<sup>36</sup> The R6G-doped SU-8 polymer microring laser clearly had better photostability than TZ-001.

Figure 8(a) indicates that the lasing peak blue-shifted by 0.182 nm upon increasing the temperature from 39 °C to 41 °C. The sensitivity of the temperature sensor was determined to be 0.0858 nm/°C by linear fitting [Fig. 8(b)]. This value was nearly one-third the sensitivity of SU-8 (see Table SI, [supplementary material](#)). The temperature resolution was estimated to be 0.35 °C. For TZ-001, the above experimental results demonstrated its low TO coefficient (physical property) and the versatility of our chip-scale sensing platform.

In our work, a high-sensitivity temperature sensor based on an R6G-doped SU-8 WGMs polymer microring laser has been developed, and its properties were characterized by a simple free-space optics measurement setup. To demonstrate the versatility of our sensing platform and to further understand the physical and mechanical properties of the hyperbranched TZ-001 polymer, R6G-doped TZ-001 as an alternative core layer material was chosen for deposition on the microring resonator host wafer. Based on the experimental results, the R6G-doped SU-8 polymer microring laser had a lower lasing threshold and better photostability compared to TZ-001, which illustrates the capability of the R6G-doped SU-8 polymer microring laser to act as a high-performance sensing element. Lastly, the sensitivities of the temperature sensors of both polymer microring lasers in the range 31–43 °C were determined to be 228.6 pm/°C and 85.8 pm/°C, respectively, and the temperature resolutions were estimated as 0.13 °C and 0.35 °C, respectively.

Several advanced features based on these proof-of-concept temperature sensors are worthy of further investigation and development. First, we will incorporate encapsulation layers to create highly photostable optofluidic microring laser temperature sensors.<sup>37</sup> In addition, we will incorporate highly

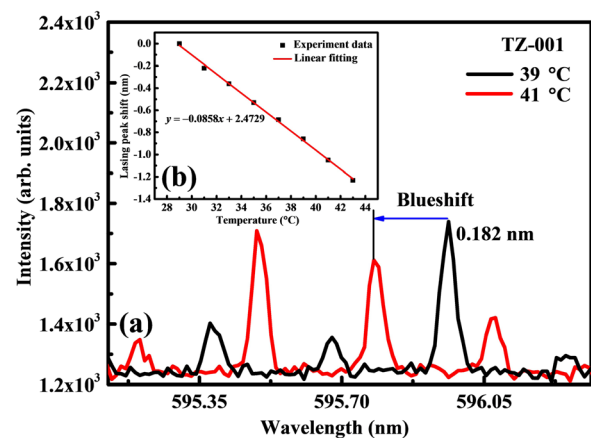


FIG. 8. (a) Lasing spectra of the R6G-doped TZ-001 polymer microring laser at 39 °C and 41 °C. (b) The inset shows the lasing peak shifts as a linear function of temperature.

reliable photonic waveguides with a high degree of freedom on the same chip.<sup>34</sup> Once the compatibility of this sensor with liquid environments is demonstrated in our future work, the rapid and simple implementation of these polymer-coated temperature sensors will further expand their adaptability in temperature sensing applications, particularly in cellular thermometry.

See [supplementary material](#) for the fabrication methods of polymer microring lasers and the description of free-space optics measurement setup.

This work was supported by the National Science Foundation (Nos. DBI-1256001 and DBI-1451127). The authors gratefully thank Q. Y. Cui and J. Zhou from the Michigan of University for experimental assistance. L.W. acknowledges C. Zhang from the National Institute of Standards and Technology (NIST) for linguistic revision. We would also like to acknowledge the technical support from Lurie Nanofabrication Facility (LNF) at the University of Michigan.

- <sup>1</sup>V. M. Lauschke, C. D. Tsiariris, P. Francois, and A. Aulehla, *Nature* **493**, 101 (2013).
- <sup>2</sup>C. Gota, K. Okabe, T. Funatsu, Y. Harada, and S. Uchiyama, *J. Am. Chem. Soc.* **131**, 2766 (2009).
- <sup>3</sup>A. Schroeder, D. A. Heller, M. M. Winslow, J. E. Dahlman, G. W. Pratt, R. Langer, T. Jacks, and D. G. Anderson, *Nat. Rev. Cancer* **12**, 39 (2012).
- <sup>4</sup>H. L. Liu, Y. Y. Fan, J. H. Wang, Z. S. Song, H. Shi, R. C. Han, Y. L. Sha, and Y. Q. Jiang, *Sci. Rep.* **5**, 14879 (2015).
- <sup>5</sup>F. Vetrone, R. Naccache, A. Zamarron, A. J. de la Fuente, F. S. Rodriguez, L. M. Maestro, E. M. Rodriguez, D. Jaque, J. G. Sole, and J. A. Capobianco, *ACS Nano* **4**, 3254 (2010).
- <sup>6</sup>Y. Y. Huang, T. Guo, Z. Tian, B. Yu, M. F. Ding, X. P. Li, and B. O. Guan, *ACS Appl. Mater. Interfaces* **9**, 9024 (2017).
- <sup>7</sup>J. G. Zhu, S. K. Ozdemir, Y. F. Xiao, L. Li, L. He, D. R. Chen, and L. Yang, *Nat. Photonics* **4**, 46 (2010).
- <sup>8</sup>C. Zhang, T. Ling, S. L. Chen, and L. J. Guo, *ACS Photonics* **1**, 1093 (2014).
- <sup>9</sup>C. Zhang, S. L. Chen, T. Ling, and L. J. Guo, *IEEE J. Lightwave Technol.* **33**, 4318 (2015).
- <sup>10</sup>H. Lee, T. Chen, J. Li, K. Y. Yang, S. Jeon, O. Painter, and K. J. Vahala, *Nat. Photonics* **6**, 369 (2012).
- <sup>11</sup>B. Peng, S. K. Ozdemir, F. C. Lei, F. Monifi, M. Gianfreda, G. L. Long, S. H. Fan, F. Nori, C. M. Bender, and L. Yang, *Nat. Phys.* **10**, 394 (2014).

- <sup>12</sup>B. Min, E. Ostby, V. Sorger, E. Ulin-Avila, L. Yang, X. Zhang, and K. J. Vahala, *Nat. Lett.* **457**, 455 (2009).
- <sup>13</sup>C. Zhang, H. Subbaraman, Q. C. Li, Z. Y. Pan, J. G. Ok, T. C. Ling, J. Chung, X. Y. Zhang, X. H. Lin, R. T. Chen, and L. J. Guo, *J. Mater. Chem. C* **4**, 5133 (2016).
- <sup>14</sup>L. H. Yu, Y. L. Yin, Y. C. Shi, D. X. Dai, and S. L. He, *Optica* **3**, 159 (2016).
- <sup>15</sup>Y. G. Zhang and Y. C. Shi, *Opt. Lett.* **40**, 264 (2015).
- <sup>16</sup>B. Ozel, R. Nett, T. Weige, G. Schweiger, and A. Ostendorf, *Meas. Sci. Technol.* **21**, 094015 (2010).
- <sup>17</sup>G. D. Kim, H. S. Lee, C. H. Park, S. S. Lee, B. T. Lim, H. K. Bae, and W. G. Lee, *Opt. Express* **18**, 22215 (2010).
- <sup>18</sup>M. S. Kwon and W. H. Steier, *Opt. Express* **16**, 9372 (2008).
- <sup>19</sup>H. Xu, M. Hafezi, J. Fan, J. M. Taylor, G. F. Strouse, and Z. Ahmed, *Opt. Express* **22**, 3098 (2014).
- <sup>20</sup>D. X. Xu, M. Vachon, A. Densmore, R. Ma, S. Janz, A. Delège, J. Lapointe, P. Cheben, J. H. Schmid, E. Post, S. Messaoudène, and J. M. Fédéli, *Opt. Express* **18**, 22867 (2010).
- <sup>21</sup>L. Zhou, K. Okamoto, and S. J. B. Yoo, *IEEE Photonics Technol. Lett.* **21**, 1175 (2009).
- <sup>22</sup>B. Guha, J. Cardenas, and M. Lipson, *Opt. Express* **21**, 26557 (2013).
- <sup>23</sup>J. Teng, P. Dumon, W. Bogaerts, H. Zhang, X. Jian, X. Han, M. Zhao, G. Morthier, and R. Baets, *Opt. Express* **17**, 14627 (2009).
- <sup>24</sup>Y. G. Zhang, P. H. Liu, S. L. Zhang, W. X. Liu, J. Y. Chen, and Y. C. Shi, *Opt. Express* **24**, 23037 (2016).
- <sup>25</sup>B. B. Li, Q. Y. Wang, Y. F. Xiao, X. F. Jiang, Y. Li, L. X. Xiao, and Q. H. Gong, *Appl. Phys. Lett.* **96**, 251109 (2010).
- <sup>26</sup>J. C. Knight, G. Cheung, F. Jacques, and T. A. Birks, *Opt. Lett.* **22**, 1129 (1997).
- <sup>27</sup>T. Wienhold, S. Kraemmer, S. F. Wondimu, T. Siegle, U. Bog, U. Weinzierl, S. Schmidt, H. Becker, H. Kalt, T. Mappes, S. Koeberaf, and C. Koos, *Lab Chip* **15**, 3800 (2015).
- <sup>28</sup>J. Yang and L. J. Guo, *IEEE J. Sel. Top. Quantum Electron.* **12**, 143 (2006).
- <sup>29</sup>L. Gounaridis, P. Groumas, E. Schreuder, R. Heideman, H. Avramopoulos, and C. Kouloumentas, *Opt. Express* **24**, 7611 (2016).
- <sup>30</sup>H. Yoshioka, T. Ota, C. Chen, S. Ryu, K. Yasui, and Y. Oki, *Sci. Rep.* **5**, 10623 (2015).
- <sup>31</sup>H. Chandralalim and X. D. Fan, *Sci. Rep.* **5**, 18310 (2015).
- <sup>32</sup>J. T. Li, Y. Lin, J. F. Lu, C. X. Xu, Y. Y. Wang, Z. L. Shi, and J. Dai, *ACS Nano* **9**, 6794 (2015).
- <sup>33</sup>H. Chandralalim, S. C. Rand, and X. D. Fan, *Appl. Opt.* **56**, 4750 (2017).
- <sup>34</sup>H. Chandralalim, S. C. Rand, and X. D. Fan, *Sci. Rep.* **6**, 32668 (2016).
- <sup>35</sup>Z. H. Liu, L. Liu, Z. D. Zhu, Y. Zhang, Y. Wei, X. N. Zhang, E. M. Zhao, Y. X. Zhang, J. Yang, and L. B. Yuan, *Opt. Lett.* **41**, 4649 (2016).
- <sup>36</sup>L. Dong, L. Liu, F. Ye, A. Chughtai, S. Popov, A. T. Friberg, and M. Muhammed, *Opt. Lett.* **37**, 34 (2012).
- <sup>37</sup>H. Chandralalim, Q. S. Chen, A. A. Said, M. Dugan, and X. D. Fan, *Lab Chip* **15**, 2335 (2015).